Neural Network-based Magnetometer Sensor Model for Virtual Magnetic-based Navigation Testbed

Aditya Penumarti*, Nikhil Iyer†, Loi Park ‡, J. Humberto Ramos§, Jane Shin ¶
University of Florida, Gainesville, Florida, 32611

Localization using magnetic anomalies is a promising approach for GPS-denied navigation, particularly in challenging environments such as indoor spaces, heavily forested areas, and long-horizon mission scenarios. However, the high cost of precision magnetometers and the complexities of calibration, influenced by distortions from both the platform and the surrounding environment, present notable challenges like wider access for the broader community and the rapid advancement of research in the field. Additionally, representative simulations of precision magnetometers are scarce, if not unavailable. However, simulating magnetic readings is not straightforward, at least not with the accuracies that GPS-denied navigation would require. Given the challenges in accurately modeling the interaction between magnetic fields and robots—particularly as current models often fall short for many applications—this paper introduces a neural network-based sensor model designed to account for environmental factors and internal and external magnetic field influences. The proposed approach also includes a virtual experimental framework implemented in NVIDIA Omniverse, providing a simulation environment where realistic, representative sensor measurements can be utilized for research and testing. This testbed is expected to serve as a tool for investigating magnetic-based navigation algorithms without requiring extensive physical setups. This testbed is released publically for researchers to access and implement novel navigation and localization architectures. [Code and Sim]

I. Introduction

Accurate and reliable localization is critical to autonomous missions involving mobile robots or vehicles. Outdoor autonomous systems typically rely on Global Positioning Systems (GPS) for localization. However, GPS signals face challenges such as jamming, signal degradation, or even complete unavailability in certain environments [1]. Various methodologies have been developed to overcome these challenges by leveraging different sensor types and alternative navigation strategies. These include, to name a few, simultaneous localization and mapping (SLAM), LiDAR-based techniques, visual-inertial odometry (VIO), and localization using ultrasonic or radar sensors [2, 3]. Nonetheless, these techniques often rely on localized salient environmental features and can quickly become less effective when the system must navigate over uniform scenes (water, forests, sand) or areas with dynamic or feature-deprived conditions.

Recent advances in GPS-denied localization have explored using Earth's magnetic anomalies for navigation and positioning, an approach known as magnetic anomaly navigation (MagNav). MagNav takes advantage of the distinctive magnetic anomalies generated by ferromagnetic materials in the Earth's crust (i.e., the crustal magnetic field) [4] to estimate a global location. This technique provides a promising alternative to GPS-based localization since magnetic anomaly sensors are difficult to jam due to the rapid signal decay over distance (requiring significant energy to disrupt), and the invariant nature of the magnetic anomalies to changing environmental conditions [5]. MagNav has been successfully implemented across various platforms, including ground [6–10] and aerial vehicles [4, 5, 11]. While MagNav is a promising solution for GPS-denied long-duration navigation, there is a significant challenge in advancing research in this domain: the high cost of total field magnetometers, which can be prohibitive for many researchers. As a result, many researchers rely on simulations before transitioning to physical testing.

A virtual testbed for MagNav research would require key components used in existing navigation approaches, including prior knowledge of the magnetic anomaly map, a motion model for pose propagation, and measurements

*Ph.D. Student, Department Mechanical and Aerospace Engineering
†Undergraduate Student, Department of Electrical and Computer Engineering
‡Undergraduate Student, Department of Mechanical and Aerospace Engineering
§Research Scientist, Department of Mechanical and Aerospace Engineering
¶Assistant Professor, Department of Mechanical and Aerospace Engineering

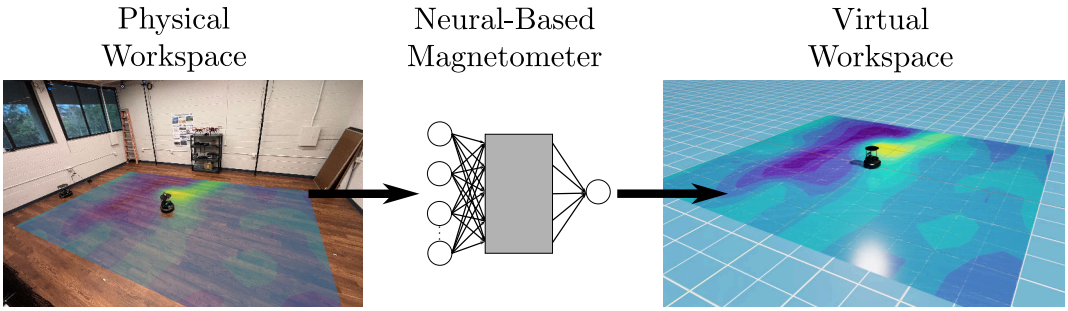

Fig. 1 Physical to virtual workspace pipeline. The physical system magnetic anomaly navigation platform was duplicated and simulated using NVIDIA's Isaac Sim. A virtual testbed enables progress in the field without the need for expensive physical setups to conduct experiments.

of the sensed magnetic intensity. With these elements, recursive estimation filters, for instance, can be applied to a virtual MagNav system for state estimation. While MagNav can be performed without a prior map [12], many practical applications are map-based, and thus, this paper focuses on map-based MagNav.

Although a magnetic map can be collected and the model of the navigating vehicle may be accurately known, it is difficult to model and thus simulate a magnetic measurement with the actual vehicle-magnetic field interaction [13, 14]. In particular, the challenge lies in how environmental and platform disturbance vector fields are measured by the magnetometer, which varies from one vehicle to another. While there exist sensor modeling approaches, such as physics-based, estimation-theoretic-based, and probabilistic models [15, 16], there still exist limitations in fully modeling the complex physical-world magnetometer for MagNav applications. Consequently, the sensor model presented here is an approximate dual of the Tolles-Lawson calibration method. While the Tolles-Lawson calibration method removes the interferences [17], the method presented here intentionally reconstructs interferences to generate the total magnetic field. This inversion establishes a complementary relationship between calibration and reconstruction, allowing many of the models and methods derived for calibration purposes to be applied here. Unfortunately, this model is insufficient for the necessary accuracy for navigation as described in [18].

Therefore this paper proposes a data-driven modeling approach to encapsulate the nuanced linear and non-linear effects that a traditional Tolles-Lawson model would not include. Specifically, a neural network is used to bypass the modeling of the magnetic field-vehicle interaction and capture the behavior of a physical total field magnetometer. The neural network approach is then virtualized using NVIDIA's Isaac Sim to make it widely available to the community

II. Problem Formulation

This paper presents the foundations for simulating a total field magnetometer measurement when such a magnetometer is attached to a small mobile robot that navigates a fixed workspace defined in two dimensions as $\mathcal{W} \subset \mathbb{R}^2 \times \mathbb{S}^1$. The simulated magnetic measurement of this work intends to emulate a measurement disturbed by 1) the environment's electromagnetic sources and 2) the robot's self-structure, including permanent, induced, and Eddy effects. Note that an accurate simulation of these effects is not straightforward because permanent, induced, Eddy, and the robot's magnetic and electromagnetic effects are often present simultaneously, and their mathematical models are only partially known. Indeed, these effects are in addition to the fact that the measurements used to fit, find, or construct a sensor model would be, in principle, noisy and already affected by the aforementioned effects. One possible way to model and simulate the permanent, induced, and Eddy effects is to use the classical calibration Tolles-Lawson model. This approach provides a base model to approximate and simulate these effects [17]. This model is relatively simple, but it has been used in practice with a high success rate [4]. The classical Tolles-Lawson magnetic measurement model assumes that the measurement reported by the magnetometer B_t is composed of the Earth field B_e, permanent disturbance B_p, induced disturbances B_i, and Eddy effects B_{ed}:

$$B_t = B_e + B_p + B_i + B_{ed} \tag{1}$$

When using the Tolles-Lawson approach, once B_p,B_i,B_{ed} are determined, often via a least-squares regression, a "clean" measurement of the Earth's field B_e can be obtained via:

$$B_e = B_t - B_p - B_i - B_{ed} \tag{2}$$

Although it would be possible to use this equation to simulate the magnetometer reading using Eq. (1) and Earth's field intensity with Eq. (2), any other additional effects present beyond B_p, B_i, B_{ed} are ignored, and the simulated sensor would be undesirably less representative of the real sensor. Adding more linear and nonlinear terms to the Tolles-Lawson equation to capture additional effects is possible. However, a better representation of the magnetic reading effects is contingent on the accuracy of such terms, which, again, are generally difficult to model or simply unknown [18]. These reasons motivate the proposed approach to simulate actual magnetic scalar readings for navigation using a data-driven approach, in turn, leading us to the following problem statement.

A. Problem Statement

Determine the magnetic disturbances via a data-driven universal function approximation, i.e., a neural network, to reproduce the disturbances that a real magnetometer would report when attached to a small vehicle. Such a simulated disturbance is given as:

$$\tilde{B}_n \approx B_p + B_i + B_{ed} + B_a \tag{3}$$

where $\tilde{B}_n$ is the simulated disturbances and B_a is any additional disturbances not accounted for by the Tolles-Lawson model.

The magnetic measurements for training, which will include the disturbance effects mentioned, are collected using a real-world platform with a high-precision scalar magnetometer. It is important to highlight that for this work, the nominal, undisturbed measurement is taken with the vehicle at rest, with all actuators disabled, and with the robot heading north. In this setting, the network's job is effectively to learn to produce the corresponding disturbance at the current heading for the current motion and in-use actuators. In this manner, per the nonlinear nature of neural networks, without specifying explicit base functions like in the Tolles-Lawson case, it can produce a disturbance that embodies more complex real-world effects of the platform.

III. Neural-Network-based Magnetometer Sensor Model

A learning-based model is employed since no simple model directly correlates platform characteristics to interference $\tilde{B}_n$. In particular, a neural network is designed to infer a relationship between platform sensor data and disturbances sensed by the total field magnetometer. While learning-based methods for interference estimation are not new to MagNav [17, 19, 20], previous works primarily focused on removing magnetic interference. In this work, the neural network predicts the magnetic disturbances generated by the platform, enabling approximate simulation of the sensor in a virtual test environment.

A. Architecture Design

1. Features

Before training, the correlation between the inputs and the desired output was calculated to determine what input-output data could be more relevant for better learning. Specifically, and given the assumed non-linear relationship between platform sensors and magnetic interferences, the Spearman rank correlation coefficient is used [21]. The results are shown in Fig. 2. This figure highlights a correlation between what is deemed relevant variables for the platform, which includes an IMU compass and gyroscope, odometry which are robot linear and angular velocities based on wheel speeds, LiDAR interference, and battery status. Among these, the ground truth angle and the compass yaw measurement exhibit the highest correlation coefficients as they provide information about the robot heading, similar to a vector magnetic reading. Lesser-correlated variables are retained in the training data to enhance robustness. The selected input

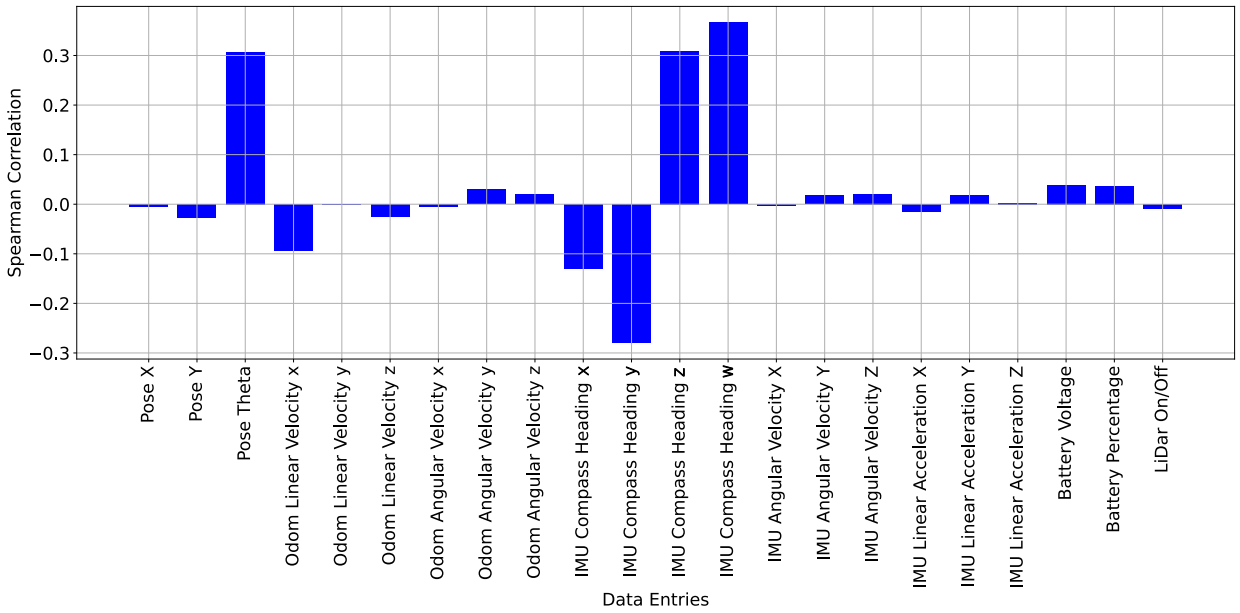

Fig. 2 Spearman correlation coefficient comparison between magnetic interference ($\tilde{B}_n$) and various inputs available for the platform.

features are,

$$\begin{bmatrix} x_1 \\ x_2 \\ x_3 \\ \vdots \\ x_{20} \end{bmatrix} = \left[\phi_G, \mathbf{V}, \boldsymbol{\omega}, \boldsymbol{\zeta}, \delta\boldsymbol{\omega}, \delta\boldsymbol{a}, \mathcal{V}_{\text{batt}}, \mathcal{P}_{\text{batt}}, L_{\text{status}}\right]^T \tag{4}$$

where ϕ_G is the ground truth yaw angle of the platform, $\mathbf{V} = \left[V_x, V_y, V_z\right]^T$ is the linear velocity vector from the platforms odometry, $\boldsymbol{\omega} = \left[\omega_x, \omega_y, \omega_z\right]$ is the angular velocity vector from the platforms odometry, $\boldsymbol{\zeta}$ is the IMU compass heading, $\delta\boldsymbol{\omega} = \left[\delta\omega_x, \delta\omega_y\delta\omega_z\right]$ is the IMU angular velocity vector, $\delta\boldsymbol{a} = \left[a_x, a_y, a_z\right]$ is the accelerometer vector, $\mathcal{V}_{\text{batt}} \in \mathbb{R}^+$ is the battery voltage, $\mathcal{P}_{\text{batt}} \in [0, 1]$ is the battery percentage, and $L_{\text{status}} \in \{0, 1\}$ is the LiDAR status where 0 is off and 1 is on.

2. Neural-network

The network is a fully connected feed-forward neural network of six layers. The network structure includes a 20-neuron input layer, four 512-neuron hidden layers, and a 1-neuron output layer. The output of the neural network y is the magnetic disturbance term $\tilde{B}_n$ in nanoTesla [nT]. The activation function used was ReLU with a 30 percent dropout to prevent the network from overfitting.

By only training to predict the disturbance term, the neural network learns the characteristic interference of the platform and produces position-invariant output. Position invariance is important for simulation because the choice of origin should not affect the simulation results. This also allows the underlying magnetic map to be updated occasionally without retraining the model. The interference is then described as the predictions from the neural network,

$$y = \tilde{B}_n. \tag{5}$$

The described network structure is illustrated in Fig. 3. Note that to produce a disturbed measurement, the neural network output can be added to the *a priori* ground-truth magnetic anomaly map at the current location of interest.

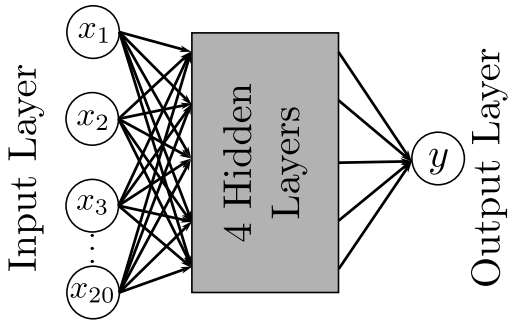

Fig. 3 Neural network model used for predicting magnetic interference. The model is a fully connected feed-forward neural network using the ReLU activation function.

B. Training

During the training, $\tilde{B}_n$ is estimated as the difference between the magnetic field intensity interpolated from the magnetic map given *a priori* and the magnetometer's total field output from the dataset sample. The model is trained using supervised learning with the standard Adam optimizer [22] and mean squared error (MSE) loss, which is represented by

$$\text{MSE} = \frac{1}{n}\sum_{i=1}^{n}(y_i - \hat{y}_i)^2 \tag{6}$$

where y_i is the target values, and $\hat{y}_i$ is the predicted target.

IV. Experimental Setup and Testbed Construction

A. Data Collection and Path Planning

The dataset and the ground-truth magnetic field map are collected at the indoor laboratory of Active Perception and Robot Intelligence Lab (APRILab) at the University of Florida using the Clearpath Robotics TurtleBot4 platform with a mounted total field magnetometer, depicted in Fig. 4. The ground truth magnetic field map is obtained using a QUSpin QTFM hybrid scalar-vector magnetometer with minimal electronic interference, while the TurtleBot4 remains stationary to mitigate induced, Eddy, and augmented magnetic disturbances from the platform during map collection. The training and test datasets are recorded over a $6\,\text{m} \times 3.5\,\text{m}$ area at varying yaw angles with a resolution of $0.25\,\text{m} \times 0.25\,\text{m} \times 90°$, enhancing the spatial detail of the map. The recorded data are interpolated using trilinear interpolation over a regular grid. The resulting ground-truth map for a 90° heading is shown in Fig. 5.

The training data is gathered using onboard sensors integrated into the Clearpath Robotics TurtleBot4 platform, which navigated along predefined paths to ensure a diverse representation of the input space. Differences in robot dynamics, sensor placements, and state data between platforms significantly impact the interference patterns observed and, consequently, the neural network's performance. Therefore the trained neural network model is only suitable for data collected from the TurtleBot4. Several structured test paths are designed to ensure a comprehensive dataset and capture diverse state scenarios Additionally, manually controlled paths are utilized to introduce variability and randomness, allowing the robot to explore a broader range of the input space beyond structured predefined paths.

Both structured and unstructured motions are considered to acquire a comprehensive and accurate representation of the input space for training. Structured motions are generated by following paths such as sine wave and lawnmower patterns, offering stable and systematic workspace coverage through diverse designs, and ensuring efficient and reliable data. On the contrary, unstructured motions are driven by manual inputs, introducing variability and randomness enabling the model to capture non-linearities. Together, these approaches provide a balanced framework for gathering data points to train the neural network.

The sine wave pathway is chosen for its ability to control a range of amplitudes and frequencies, granting access to various regions of the map for data collection. Moreover, the curvilinear nature of sine waves ensured smoother, more predictable robot dynamics. The paths are modeled using the following function:

$$y = A\sin(\omega x - x_0) + y_0 \tag{7}$$

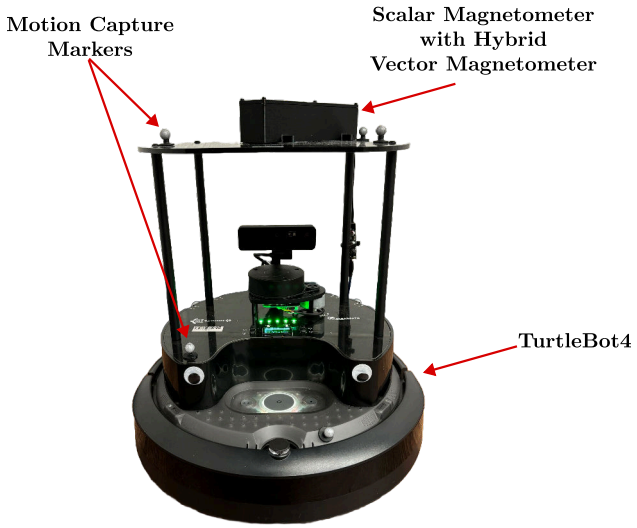

Fig. 4 Clearpath TurtleBot4 with motion capture markers and a total field magnetometer.

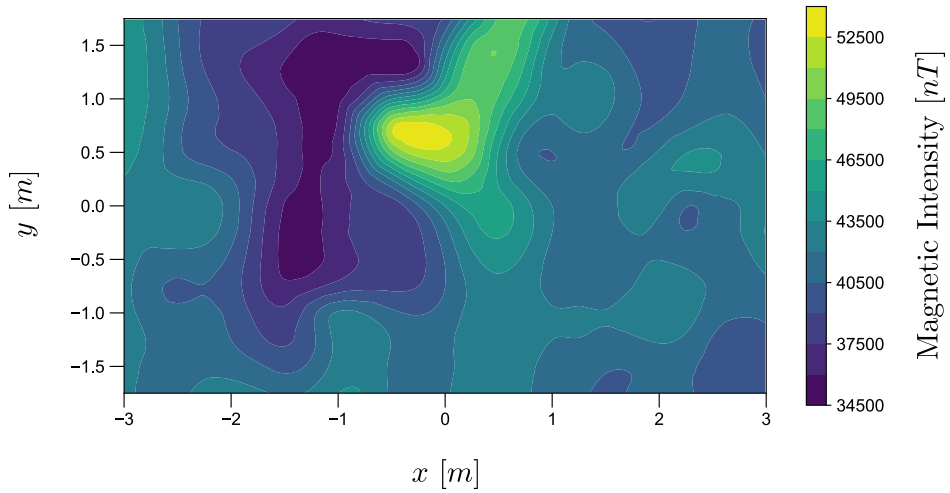

Fig. 5 Magnetic anomaly map collected indoors at the Active Perception and Robot Intelligence Lab (APRILab) at the University of Florida. The map was collected at $0.25\,\mathrm{m} \times 0.25\,\mathrm{m}$ **grid space.**

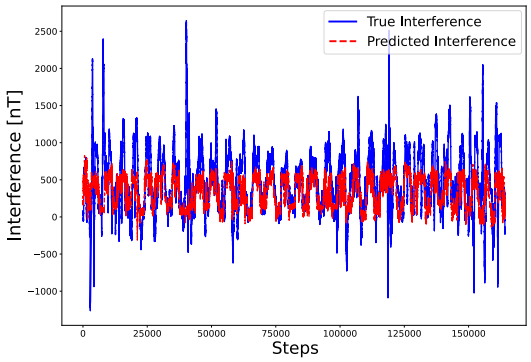

(a) Magnetic interference performance with a full input vector

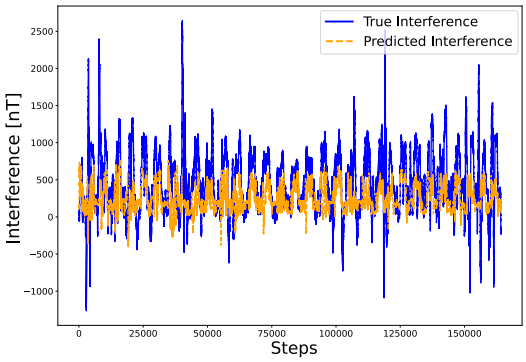

(b) Magnetic interference performance with a partial input vector

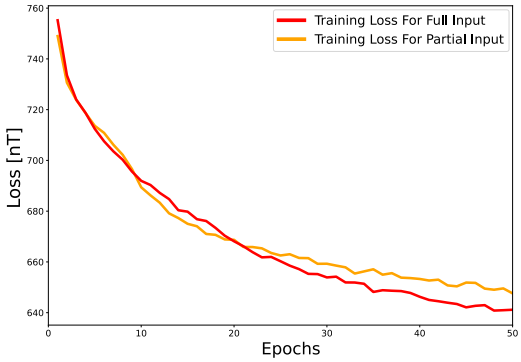

(c) Training Loss

Fig. 6 (a) Prediction performance comparison for a model utilizing the full input vector, which includes lowly correlated data for improved robustness. The mean absolute error (MAE) for this evaluation is 284.631 nT. (b) Prediction performance comparison for a model using only highly correlated values from the input vector. The MAE for this evaluation is 338.814 nT. (c) Training loss comparison between the two models. The results indicate better training loss performance with the full input vector, as evidenced by the significantly lower MAE compared to the model with only highly correlated inputs

where A represents the desired amplitude of the sine wave, ω is the desired wave frequency, $x \in \mathcal{W}$ corresponds to the x coordinates, and $y \in \mathcal{W}$ corresponds to the y coordinates.

The lawnmower path employs a systematic back-and-forth motion, offering an efficient and comprehensive approach to data collection. The path ensures complete corner-to-corner coverage of the workspace by traversing every segment consistently. The path's scalability makes it adaptable to various map sizes and shapes, particularly rectangular workspaces. The lawnmower path can be described as follows:

$$\mathbf{r} = f(a_0, a_e, h, \delta_{step}) \tag{8}$$

where $\mathbf{r}$ is the vector containing the points on the path, f is the function generating the lawnmower path, a_0 and a_e are the initial and final coordinates along the axis of traversal, h is the height of the path along the perpendicular axis, and δ_{step} is the step size between each parallel line segment.

An unstructured path is incorporated into the dataset to ensure the robustness of the model through manual operation. Unlike structured paths that may encourage overfitting and capture only the mean of the input space, unstructured motion introduces randomness to the collected data. By varying linear and angular velocities, the randomness from human control diversifies the dataset and trains the neural network to recognize and handle a broader range of scenarios. This approach reduces the bias from repetitive patterns, enabling the network to better adapt to real-world variability and complexities.

B. Isaac Sim Setup

For the virtual testbed, NVIDIA's Isaac Sim is employed to simulate the magnetometer within a controlled and repeatable environment, facilitating detailed system testing. Isaac Sim is selected for its advanced dynamics simulation capabilities, broad accessibility, seamless integration with the Robot Operating System (ROS) for creating digital twins, and its potential for expansion into reinforcement learning applications. The Clearpath TurtleBot4 model is imported into the simulation environment, with its dynamics tuned based on known physical parameters. The system, including its full articulation tree, which describes the joint motions and relations between each link in the platform, is placed in a workspace that mirrors the physical world model corresponding to the specific platform used in this study.

An IMU is imported within the virtual testbed to provide data to the neural network, ensuring realistic sensor outputs. The battery state is modeled as a linear decay function, decreasing with each simulation loop. Voltage fluctuations are simulated as a zero-mean Gaussian noise centered around a user-defined mean, accurately reflecting real-world conditions.

The system is integrated with ROS 2, enabling real-time feature output for model evaluation. This integration allows the neural network to publish total field values as ROS 2 messages, providing users with seamless access to the data for incorporation into custom implementations. Input data for the network is received from ROS 2 messages, which publish each feature in simulation time, facilitating efficient evaluation within the simulation framework.

V. Results

The proposed neural network model is trained and tested in real-time in physical and virtual environments, utilizing onboard sensors to simulate magnetometer interference. This simulated interference is added to B_e to compute the total magnetic magnitude, B_t. The trained neural network is evaluated along several test paths, A through E, and presented in Table. 1. The table compares MAE loss to the naive loss which is the simple mean of the training data.

Table 1 Comparison of Magnetic Interference Performance for Different Test Cases

Test Case	Path Types	Loss	Naive Loss
A	High Frequency Sine Wave	217.6165	225.1818
B	Curvilinear Run #1	307.8796	407.1321
C	Curvilinear Run #2	267.0007	381.4163
D	Lawmower with a Y-axis Split	284.6316	333.0688
E	Narrow Figure 8	323.6039	409.3078

Test cases C and D, conducted on the physical platform and exhibiting significant variations in the coverage of the input space, are plotted alongside the ground truth interference in Fig. 7. The figure demonstrates that the neural

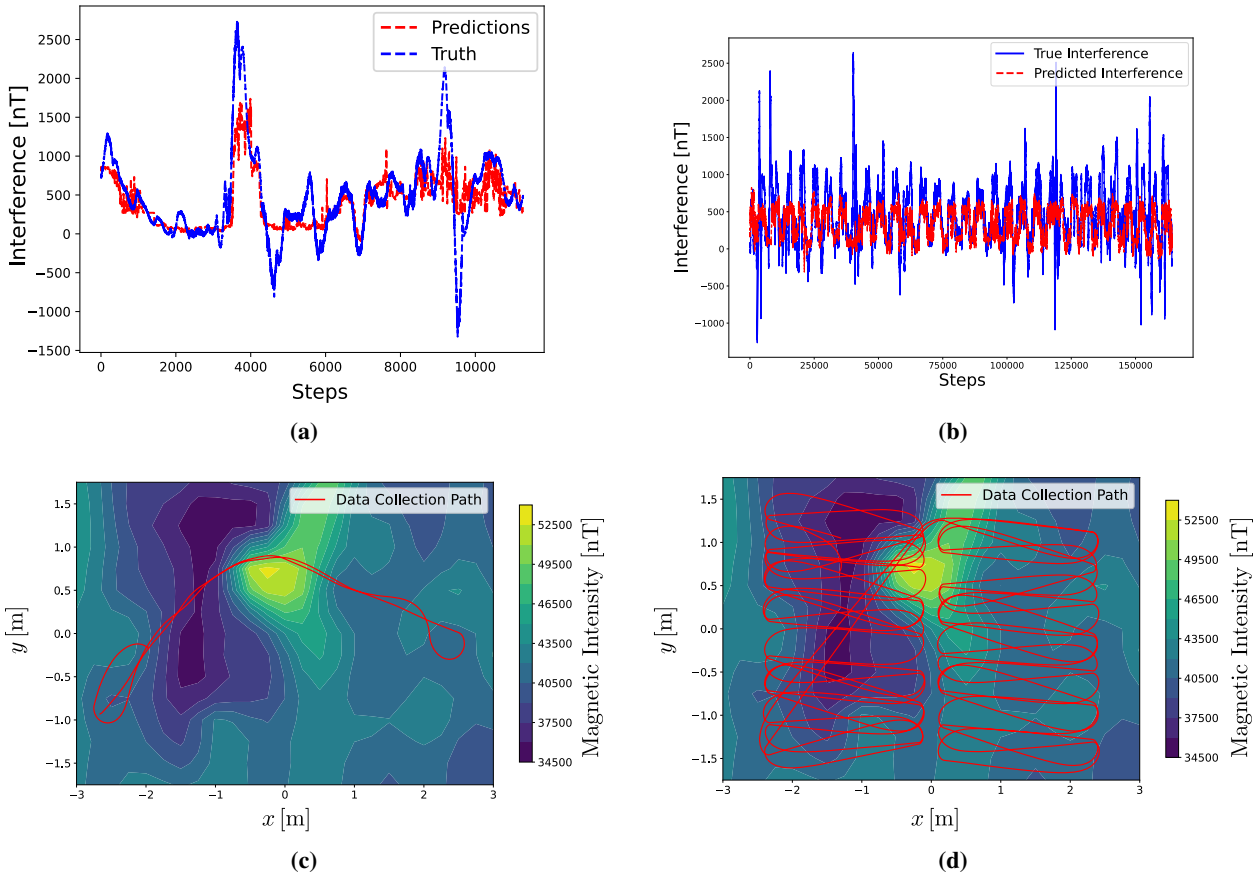

Fig. 7 (a) Test case C's model predictions are evaluated against the true interference. The true interference was calculated by subtracting the total field from the map. (b) Test case D's model predictions compared to true interference. (c) Visualization of the path followed by the platform in test case C. (d) Visualization of the path followed by the platform in test case D.

network effectively captures magnetic interferences. However, discrepancies are observed in fully predicting the extent of the interference, primarily attributed to the absence of vector field data.

The network is further compared by running it in both simulated and physical environments. By completing identical paths with the LiDAR off and battery state set similarly, similar features are generated in both environments. The network performance with the resulting total magnetic field across both environments is presented in Fig. 8. The neural network outputs closely matched the expected values in both cases, demonstrating consistency between the physical and simulated implementations.

VI. Discussion

The results show that the neural network successfully captures magnetic interferences, outperforming the baseline method that uses the mean of the training dataset. As demonstrated in Table 1, the mean absolute error (MAE) for the neural network is considerably lower, indicating its ability to generalize and identify patterns beyond the average behavior of the training data. However, despite the neural network's superior performance compared to the mean baseline, some errors persist, particularly in predicting the full scope of interference. These inaccuracies are primarily due to the lack of vector field measurements, which would offer additional information necessary to resolve complex interference patterns. Additionally, oscillating disturbances from onboard electronics, such as LiDAR, are challenging to distinguish without vector field measurements, which leads to the mean value generating a fairly similar prediction to the neural network in some cases.

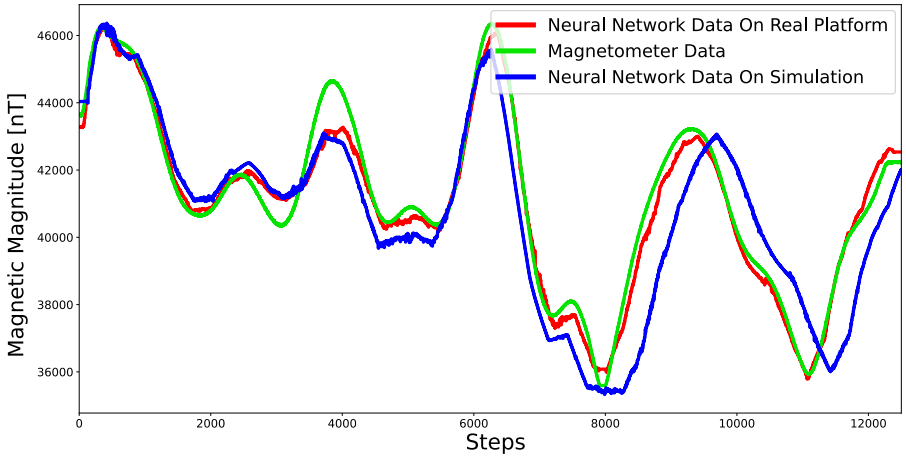

Fig. 8 Comparison of neural network predictions in simulation and physical environments. The figure shows the predicted magnetic magnitude from the total field magnetometer, with the ground truth total field included for reference. A distinct time-shift is observed towards the latter end of the plot, attributed to slight differences in platform speed between simulation and reality.

The performance is further analyzed over two distinct paths: a simple map traversal and a coverage path using a lawnmower trajectory. In both cases, the predictions from the neural network closely align with the ground truth interference derived from the total field data. Notably, the lawnmower trajectory, designed for systematic and distinctly abrupt movements, enables the model to capture more nuanced disturbances than the simple traversal. Despite this, certain regions still exhibit larger prediction errors, likely due to unobserved environmental factors or dataset uniformity.

A comparison of the simulated and physical implementations of the system (Fig. 8) reveals a high degree of consistency between the two environments. The platforms in both environments are identical since the neural network is trained exclusively on data from a single platform, making the model specifically applicable to the Clearpath TurtleBot4. The platform follows identical paths using the same controller in both environments. This result underscores the effectiveness of the virtual testbed in replicating real-world conditions for magnetic interference modeling. However, a distinct time-shift is observed towards the latter end of the plot, attributed to slight differences in platform speed between simulation and reality. The time shift can be eliminated with further tuning. These findings suggest that while simulation provides a robust tool for pre-deployment testing, fine-tuning with physical data remains essential for accurate modeling.

The experiments highlight the neural network's potential to approximate magnetometer interference using readily available onboard sensors. This approach provides a scalable alternative to traditional methods requiring vector field measurements, which are challenging to simulate and deploy in indoor environments. However, further work is necessary to address the observed prediction errors, potentially by including additional features, improved data collection strategies, or advanced model architectures. Future efforts should focus on enriching the training dataset with more diverse scenarios, including dynamic changes in the environment and platform. Incorporating techniques such as hybrid approaches that combine data-driven learning with physics-based models could provide more accurate and interpretable predictions.

VII. Conclusion

The proposed neural network model demonstrates an advancement in bridging the simulation-to-reality gap for magnetic interference, outperforming the traditional naive mean. By capturing platform-specific noise and nuanced interference patterns, this approach offers an enhanced model for magnetic disturbances that can account for subtle non-linearities. However, the results also reveal a limitation: the absence of vector field measurements in the input layer considerably impacts the model's performance compared to literature where such data is incorporated, highlighting the need for a more comprehensive simulation.

Using a dynamics simulator tailored to the specific platform on which the neural network was trained, further

validates the realism of the virtual testbed. The similarity between the virtual and physical environments enables researchers to effectively test algorithms and methods using the simulated magnetometer, eliminating the high costs of acquiring a physical total field magnetometer, at least for early MagNav-related prototypes. Additionally, this simulation framework supports scalability, allowing researchers to simulate multiple platforms and sensors without the financial and logistical burdens of additional hardware, and explore repeated training methods for advanced reinforcement learning techniques.

While the presented method offers marked improvements, further enhancements are necessary to achieve a more robust virtual model for a total field magnetometer. Integrating a simulated vector magnetometer model is expected to reduce network loss and improve evaluation performance. This extension will strengthen the simulation environment, offering greater utility for research and development in magnetic anomaly navigation and related fields.

Acknowledgments

This research was partially sponsored by the Air Force Research Laboratory under contract FA8651-22-F-1052.

References

[1] Ioannides, R. T., Pany, T., and Gibbons, G., "Known Vulnerabilities of Global Navigation Satellite Systems, Status, and Potential Mitigation Techniques," *Proceedings of the IEEE*, Vol. 104, No. 6, 2016, pp. 1174–1194. https://doi.org/10.1109/JPROC.2016.2535898, URL https://ieeexplore.ieee.org/document/7442783, conference Name: Proceedings of the IEEE.

[2] Kumar, D., and Muhammad, N., "A Survey on Localization for Autonomous Vehicles," *IEEE Access*, Vol. 11, 2023, pp. 115865–115883. https://doi.org/10.1109/ACCESS.2023.3326069, URL https://ieeexplore.ieee.org/abstract/document/10287946, conference Name: IEEE Access.

[3] Ramos, J. H., Ganesh, P., Warke, W., Volle, K., and Brink, K., "REEF Estimator: A Simplified Open Source Estimator and Controller for Multirotors," *2019 IEEE National Aerospace and Electronics Conference (NAECON)*, 2019, pp. 606–613. https://doi.org/10.1109/NAECON46414.2019.9058099.

[4] Canciani, A., "Absolute Positioning Using the Earth's Magnetic Anomaly Field," *Theses and Dissertations*, 2016. URL https://scholar.afit.edu/etd/251.

[5] Canciani, A., and Raquet, J., "Airborne Magnetic Anomaly Navigation," *IEEE Transactions on Aerospace and Electronic Systems*, Vol. 53, No. 1, 2017, pp. 67–80. https://doi.org/10.1109/TAES.2017.2649238, URL https://ieeexplore.ieee.org/document/7808987, conference Name: IEEE Transactions on Aerospace and Electronic Systems.

[6] Storms, W., Shockley, J., and Raquet, J., "Magnetic field navigation in an indoor environment," *2010 Ubiquitous Positioning Indoor Navigation and Location Based Service*, 2010, pp. 1–10. https://doi.org/10.1109/UPINLBS.2010.5653681, URL https://ieeexplore.ieee.org/document/5653681.

[7] Shockley, J., "Ground Vehicle Navigation Using Magnetic Field Variation," *Theses and Dissertations*, 2012. URL https://scholar.afit.edu/etd/1156.

[8] Anderson, M. L., Mockel, W., Sheldon, J., Francomb, A., Olson, Z., Falcon, A., Briggs, H. C., Ramos, J. H., and Waters, K. L., "Subsurface Unexploded Ordnance Detecting Robot for the Airfield Damage Repair Mission," *AIAA SCITECH 2024 Forum*, 2024, p. 2089.

[9] Deshpande, M., Majji, M., and Ramos, J. H., "Magnetic Field Aided Vehicle Localization with Acceleration Correction," *arXiv preprint arXiv:2411.06543*, 2024.

[10] Ramos, J. H., Shin, J., Volle, K., Buzaud, P., Brink, K., and Ganesh, P., "Information-Aware Guidance for Magnetic Anomaly based Navigation," *2022 IEEE/RSJ International Conference on Intelligent Robots and Systems (IROS)*, IEEE, 2022, pp. 6347–6354.

[11] Canciani, A. J., "Magnetic Navigation on an F-16 Aircraft Using Online Calibration," *IEEE Transactions on Aerospace and Electronic Systems*, Vol. 58, No. 1, 2022, pp. 420–434. https://doi.org/10.1109/TAES.2021.3101567, conference Name: IEEE Transactions on Aerospace and Electronic Systems.

[12] Lee, T. N., and Canciani, A. J., "MagSLAM: Aerial simultaneous localization and mapping using Earth's magnetic anomaly field," *NAVIGATION: Journal of the Institute of Navigation*, Vol. 67, No. 1, 2020, pp. 95–107. https://doi.org/10.1002/navi.352, URL https://navi.ion.org/content/67/1/95, publisher: Institute of Navigation Section: Original Article.

[13] Group, N. A. M. A., Bankey, V., Cuevas, A., Daniels, D. L., Finn, C. A., Hernandez, I., Hill, P. L., Kucks, R., Miles, W., Pilkington, M., Roberts, C., Roest, W., Rystrom, V., Shearer, S., Snyder, S. L., Sweeney, R. E., and Velez, J., "Magnetic anomaly map of North America," Tech. rep., U.S. Geological Survey, 2002. https://doi.org/10.3133/70211067, URL https://pubs.usgs.gov/publication/70211067, publication Title: Special Map.

[14] Ramos, J. H., Shin, J., Volle, K., Buzaud, P., Brink, K., and Ganesh, P., "Information-Aware Guidance for Magnetic Anomaly based Navigation," *2022 IEEE/RSJ International Conference on Intelligent Robots and Systems (IROS)*, IEEE, Kyoto, Japan, 2022, pp. 6347–6354. https://doi.org/10.1109/IROS47612.2022.9981709, URL https://ieeexplore.ieee.org/document/9981709.

[15] Ferrari, S., and Wettergren, T. A., *Information-driven planning and control*, MIT Press, 2021.

[16] Shin, J., Chang, S., Weaver, J., Isaacs, J. C., Fu, B., and Ferrari, S., "Informative multiview planning for underwater sensors," *IEEE Journal of Oceanic Engineering*, Vol. 47, No. 3, 2022, pp. 780–798.

[17] Gnadt, A. R., Wollaber, A. B., and Nielsen, A. P., "Derivation and Extensions of the Tolles-Lawson Model for Aeromagnetic Compensation," , Dec. 2022. https://doi.org/10.48550/arXiv.2212.09899, URL http://arxiv.org/abs/2212.09899, arXiv:2212.09899.

[18] Ramos, J. H., Waters, K. L., Dorr, A., Volle, K., Ganesh, P., and Brink, K., "Ownship Calibration for Indoor Magnetic Navigation," *AIAA SCITECH 2024 Forum*, Orlando, FL, 2024. https://doi.org/10.2514/6.2024-1177, URL https://arc.aiaa.org/doi/abs/10.2514/6.2024-1177, _eprint: https://arc.aiaa.org/doi/pdf/10.2514/6.2024-1177.

[19] Laoué, N., Lepers, A., Deletraz, L., and Faure, C., "Neural Network Calibration of Airborne Magnetometers," *2023 IEEE 10th International Workshop on Metrology for AeroSpace (MetroAeroSpace)*, 2023, pp. 37–42. https://doi.org/10.1109/MetroAeroSpace57412.2023.10189964, URL https://ieeexplore.ieee.org/document/10189964, iSSN: 2575-7490.

[20] Hezel, M., "Improving Aeromagnetic Calibration Using Artificial Neural Networks," *Theses and Dissertations*, 2020. URL https://scholar.afit.edu/etd/3589.

[21] Spearman, C., "The Proof and Measurement of Association between Two Things," *The American Journal of Psychology*, Vol. 15, No. 1, 1904, pp. 72–101. https://doi.org/10.2307/1412159, URL https://www.jstor.org/stable/1412159, publisher: University of Illinois Press.

[22] Kingma, D. P., and Ba, J., "Adam: A Method for Stochastic Optimization," , Jan. 2017. https://doi.org/10.48550/arXiv.1412.6980, URL http://arxiv.org/abs/1412.6980, arXiv:1412.6980.